NUMERICAL SIMULATION OF FILM COOLING EFFECTIVENESS IN A ROTATING BLADE AT HIGH BLOWING RATIOS

Nabeel Alzurfi[1, 2, *], Ali Turan[1], Adel Nasser[1], and Ahmed Alhusseny[1, 2]
*Author for correspondence
[1]School of Mechanical, Aerospace, and Civil Engineering, University of Manchester, Manchester, M13 9PL, UK,
[2]Mechanical Engineering Department, College of Engineering, University of Kufa, Najaf, Iraq,
E-mail: nabeel.al-zurfi@manchester.ac.uk

ABSTRACT

The film-cooling performance in a low-speed rotor blade of a 1-1/2 turbine stage has been examined using LES approach. Two rows of film holes were positioned on the rotor blade surface, one on the pressure surface and the other one the suction surface, with axial locations of 24.2% and 22.6% of the chord length, respectively. Each row has three cylindrical film-cooling holes with a diameter (D) of 4 mm and a tangential injection angle of 28° on the pressure side and 36° on the suction side. The Reynolds number, based on the mainstream velocity of the turbine outlet and axial length of the turbine, was fixed at $Re=1.92\times10^5$, the coolant-to-mainstream density ratio (DR) was about 2.0, and the speed of the rotor blade was taken to be 1800 rpm. Several blowing ratios (BR) in the range of 1.0–5.0 were investigated. The effects of blowing ratio, rotation, and curved surfaces were analysed to investigate the effects of the stator–rotor interaction on the film-cooling characteristics. The commercial CFD code STAR-CCM+ was used to run the simulations using the WALE subgrid-scale model for modelling the turbulence. The solutions were obtained by solving the incompressible, 3D Navier–Stokes equations under the rotating coordinates system with the energy equation, and the pressure–velocity coupling was achieved by using the well-known SIMPLE algorithm. The results show that on the pressure side, the film coverage and film-cooling effectiveness increase with increasing BR. A lower BR results in stronger film deflection. The film injection with higher BR produces better film attachment. The film deflects centripetally due to the effect of rotation. On the suction side, the trend of film coverage and film-cooling effectiveness is parabola as the blowing ratio rising and a centripetal deflection of the film is observed. The deflection of the film path could be amplified by decreasing the BR.

KEYWORDS: *Rotor blade, Large eddy simulation, Film-cooling effectiveness.*

NOMENCLATURE

C_L	[mm]	Turbine axial length
C_s	[-]	Smagorinsky model constant
C_w	[-]	WALE model constant
D	[mm]	Film hole diameter at inlet
DR	[-]	Density ratio
H	[mm]	Radial distance from the film hole
k	[$W.m^{-1}.K^{-1}$]	Thermal conductivity
L	[mm]	Length of film injection hole
BR	[-]	Blowing ratio
P	[$N.m^{-2}$]	Pressure
Pr	[-]	Prandtl Number
Pr_t	[-]	Turbulent Prandtl number
PS	[-]	Pressure side or surface
Re	[-]	Chord Reynolds number
S	[mm]	Distance along blade surface
SGS	[-]	Subgrid-scale
SS	[-]	Suction side or surface
T	[K]	Local fluid temperature
T_w	[K]	Local wall temperature
T_{aw}	[K]	Local adiabatic wall temperature

Special characters

Δ	[mm]	Filter width
η	[-]	Local film-cooling effectiveness
ρ	[kg/m^3]	Density
μ	[$N{\cdot}s/m^2$]	Dynamic viscosity
μ_t	[$N{\cdot}s/m^2$]	Subgrid-scale turbulent viscosity
ν	[m^2/s]	Kinematic viscosity
ν_t	[m^2/s]	Subgrid-scale eddy viscosity
Ω	[rad/s]	Angular velocity
β	[1/K]	Coefficient of thermal expansion

Subscripts

c	Coolant
CFL	Courant Friedrichs Lewy
∞	Free stream

Mathematical Accents

-	Filtered (LES) quantity
`	Fluctuating quantity
< >	Time averaging

INTRODUCTION

Modern gas turbine engines are designed to operate at high inlet temperatures (1800-2000 K) to improve thermal efficiency and power output. This temperature range, which is far beyond the allowable metallurgical temperatures limit, leads the turbine components to experience high heat loads and thermal stresses, which may result in material failure. Therefore, turbine blades cooling techniques have to be employed in order to increase the component life and reduce maintenance costs. To overcome the heat load, several internal cooling technologies have been applied. Besides these internal cooling technologies, film-cooling is commonly used in the real gas turbine engine. In film cooling, coolant air is injected through discrete holes drilled at several locations on the blade

exterior surface. This technique provides a protective film layer which protects the outside surface of the blade from the hot combustion gases. The performance of the film-cooling is determined by many critical flow and geometric parameters such as the mainstream Reynolds number, blowing ratio, coolant-to-mainstream density ratio, injection angle, rotating speed, turbulence intensity, surface curvature, the shape, size and location of the film hole and so on. Thus, a considerable number of investigations [1–7] have been conducted to achieve a comprehensive understanding of the film-cooling process, as well as to optimise the design of the film-hole configurations that can provide better protection with a smaller amount of coolant. Several studies [8-15] have been carried out over the past few decades on the field of a jet in a cross-flow (JICF). Initially, various researches on the cylindrical film-cooling hole have been performed to investigate effects of length and diameter of film holes, blowing ratio, injection angle on film-cooling performance. It was found that the interaction between the coolant jet and mainstream flow results in the formation of highly complex counter-rotating vortex pairs (CRVPs) near the wall surface, and the mixing process is controlled by the dynamics of these vortices. These vortices are detrimental to film cooling and known as the main contributor to the dramatic decrease in the film-cooling effectiveness because they have two undesirable effects. Firstly, the hot mainstream air is forced to enter beneath the coolant jet, thus heating the blade surface. Secondly, these vortices tend to lift the coolant jet off the surface which diminishes the film-cooling and therefore causes a reduction in the film-cooling effectiveness.

Many numerical and experimental studies on stationary film-cooling have been carried out over the past few decades. A comprehensive, detailed compilation of the film-cooling characteristics of different models has been produced by Han et al. [16]. Only a few studies of rotating-turbine conditions are available in open literature. Garg [17] computed the adiabatic film-cooling effectiveness and heat-transfer coefficient on a rotating turbine blade rotates at 5200 rpm. He found that the rotating blade produces higher adiabatic effectiveness compared with that observed for a stationary one. In a subsequent study, the same author [18] used Wilcox's k-ω turbulence model to predict the heat-transfer coefficient on a high-pressure turbine blade rotating at 11,570.2 rpm. The results showed that the heat-transfer coefficient on the cooled, isothermal blade is found to be high in the tip region, and in the leading-edge region between the hub and blade mid-span. The effectiveness over the cooled, adiabatic blade is the lowest in these regions.

The heat-transfer coefficient and film-cooling effectiveness distributions on a rotating blade in a 1-1/2 turbine stage have been carried out by different numerical and experimental studies. Yang et al. [19] investigated the effects of rotating speed and blowing ratio on film-cooling effectiveness and heat transfer coefficient for three different rotating speeds: 2400 rpm, 2550 rpm and 3000 rpm with the overall blowing ratio varying from 0.5 to 2.0. The results indicated that increasing the rotating speed leads to an increase in heat-transfer coefficient and a drop in film-cooling effectiveness. Three years later, Tao et al. [20] measured the film-cooling effectiveness using the thermochromic liquid crystal (TLC) technique. Measurements were made at three different rotating speeds of 600 rpm, 667 rpm and 702 rpm, with the blowing ratio varying from 0.3 to 3.0. Results showed that the film-cooling effectiveness increases with the blowing ratio on the pressure side while it is parabolic on the suction side. Both the film coverage and cooling effectiveness decrease with increasing rotating speed. In a recent study, Al-Zurfi and Turan [21] used LES method to examine the effects of rotation on film-cooling effectiveness and heat-transfer coefficient distributions. Their results indicated that film-cooling effectiveness increases with an increase in the rotating speed. Higher turbine rotating speed shows increased local film-cooling effectiveness spread over the pressure surface. The results also showed that the Nusselt number on the suction surface increases slightly with increasing rotating speed. On the pressure surface, at low rotating speed the Nusselt number increases rapidly as rotating speed increases, whereas it decreases slightly with an increase in rotating speed above 250 rpm.

Very little researches can be found in the open literature to study the effect of stator–rotor interaction on the film-cooling effectiveness of the rotor blade in a complete turbine stage. In this study, to the best of the authors' knowledge, LES results for a low-speed 1.5 turbine stage are presented for the first time in the open literature. The present study is a continuation of the authors' previous work [21], and focuses on the combined effects of the blowing ratio and rotation number on a film-cooled rotor blade in a low-speed 1.5 turbine stage with three film-cooling cylindrical holes on both the pressure surface (PS) and suction surface (SS) using the LES method. The results of the film-cooling effectiveness distributions over the blade surface will be helpful in understanding the physical phenomena regarding the film-cooling and beneficial in designing more efficiently cooled turbine rotor blades.

MATHEMATICAL FORMULATION

In DNS, all turbulent scales have to be resolved. In LES, on the other hand, only the large scales (resolved scales) are solved in a time-dependent simulation that uses a set of filtered equations, while the small scales (residual or subgrid-scales) are modelled via a subgrid-scale model (SGS). The LES equations in tensor notations for a three-dimensional, time-dependent, and incompressible fluid are expressed as follows:

- Continuity equation:

$$\frac{\partial \rho}{\partial t}+\frac{\partial}{\partial x_i}(\rho \bar{u}_i)=0 \qquad \in \{1,2,3\} \tag{1}$$

- Momentum equations:

$$\frac{\partial}{\partial t}(\rho \bar{u}_i)+\frac{\partial}{\partial x_j}(\rho \bar{u}_i \bar{u}_j)=-\frac{\partial \bar{p}}{\partial x_i}+\frac{\partial}{\partial x_j}(\sigma_{ij}-\tau_{ij})- \rho \varepsilon_{ikj}\varepsilon_{jlm}\Omega_k \Omega_l X_m - 2\rho \varepsilon_{ikj}\Omega_k \bar{u}_j \tag{2}$$

-Energy equation:

$$\frac{\partial}{\partial t}(\rho \bar{T})+\frac{\partial}{\partial x_i}(\rho \bar{T} \bar{u}_i)=\frac{\partial}{\partial x_i}\left(\frac{\mu}{\mathrm{Pr}}\frac{\partial \bar{T}}{\partial x_i}-\rho q_i\right) \tag{3}$$

where $\bar{u}_i$ is the resolved velocity in the i-direction (i=1,2, and 3 correspond to the x-, y- and z- directions), $\bar{p}$ is the filtered pressure, Ω is the angular velocity, ε_{ijk} is the Levi-Civita alternating tensor, $\bar{T}$ is the filtered temperature, σ_{ij} is the stress tensor due to molecular viscosity, τ_{ij} is the subgrid-scale stress and q_i is the subgrid-scale heat flux, as defined by the following equations:

$$\sigma_{ij} \equiv \left(\mu \left(\frac{\partial \bar{u}_i}{\partial x_j} + \frac{\partial \bar{u}_j}{\partial x_i} \right) - \frac{2}{3} \mu \frac{\partial \bar{u}_k}{\partial x_k} \delta_{ij} \right)$$

$$\tau_{ij} \equiv \rho \overline{u_i u_j} - \rho \bar{u}_i \bar{u}_j$$

$$q_i \equiv \overline{T u_i} - \bar{T} \bar{u}_i$$

The SGS turbulent stress term resulting from the filtering operation is unknown, and requires modelling. The SGS turbulence model employs the eddy-viscosity assumption or the Boussinesq hypothesis (Hinze, [22]) as in the RANS models and therefore the SGS stress can be computed from the following:

$$\tau_{ij} - \frac{1}{3} \delta_{ij} \tau_{kk} = -2 \mu_t \bar{S}_{ij} \qquad 4$$

where μ_t is the subgrid-scale turbulent viscosity. The isotropic part of the subgrid-scale stresses τ_{kk} is not modelled, but is added to the filtered static pressure term. The rate of strain tensor for the resolved scale is represented by $\bar{S}_{ij}$ and is defined by the following expression:

$$\bar{S}_{ij} = \frac{1}{2} \left(\frac{\partial \bar{u}_i}{\partial x_j} + \frac{\partial \bar{u}_j}{\partial x_i} \right)$$

In this study, the effects of the small scales that appear in the SGS turbulent stress term are modelled by using the wall-adapting local eddy viscosity (WALE) model [23]. The WALE model is based on the square of the velocity gradient tensor and represents the near-wall behaviour more accurately than the classical Smagorinsky model [24]. In the WALE model, the SGS turbulent viscosity becomes:

$$\mu_t = \rho L_s^{\,2} \frac{(S_{ij}^d S_{ij}^d)^{3/2}}{(\bar{S}_{ij} \bar{S}_{ij})^{5/2} + (S_{ij}^d S_{ij}^d)^{5/4}} \qquad 5$$

where L_s and S_{ij}^d are defined, respectively, as:

$$L_s = \min(\kappa y, C_w \Delta)$$

$$S_{ij}^d = \frac{1}{2} \left(\bar{g}_{ij}^2 + \bar{g}_{ji}^2 \right) - \frac{1}{3} \delta_{ij} \bar{g}_{kk}^2$$

where κ is the von Karman constant, y is the wall distance, C_w is the model coefficient, Δ is the filler width, δ_{ij} is the Kronecker delta, and $\bar{g}_{ij} = \frac{\partial \bar{u}_i}{\partial x_j}$.

The value of C_w =0.544 has been found to yield satisfactory results for a wide range of flow. The filter width can be defined as $\Delta = V^{1/3}$, with V denoting the volume of a computational cell, which yields a filter width of $\Delta = (\Delta x \Delta y \Delta z)^{1/3}$.

The SGS heat flux vector (q_i) is related to the resolved temperature field through SGS eddy diffusivity as:

$$q_i = -\alpha_t \frac{\partial \bar{T}}{\partial x_i}$$

Where $\alpha_t = \frac{\nu_t}{\mathrm{Pr}_t}$ is the SGS eddy diffusivity, ν_t is the SGS eddy viscosity, and Pr_t is the turbulent Prandtl number.

The third and fourth terms on the right-hand side of Eq.2 are the centrifugal force and Coriolis force contributions; more information is given in the authors' previous works [21, 25, 26, 27, 28].

PHYSICAL MODEL

The present film-cooling investigation is carried out for 1.5 turbine stages, which include the first-stage stator, the first-stage rotor and the second-stage stator, as shown in Fig.1. Both the stator and rotor blades have the same blade profiles and configurations, which is exactly the same as the experimental blade used by Tao et al. [20]. In their experiment, the 1.5-turbine stages include 54 blades in total. 18 blades are used in both the first- and second-stage stators with a chord of 124.5 mm and a height of 100 mm, and 18 blades in the first-stage rotor with a chord of 124.3 mm and a height of 99 mm. The rotor blade tip clearance is 1 mm, corresponding to 1.01% of the blade span. In order to significantly reduce the CPU time and computer memory requirements, it is necessary to simulate only one flow passage with periodic boundary conditions in the circumferential direction. Two rows of film holes are placed on the rotor blade surface, one each on the pressure and suction surfaces, with axial locations of 24.2% and 22.6% of the chord length, respectively. Each row has three film-cooling cylindrical holes with a diameter (D) of 4 mm and spanwise spacing of 12 mm, which gives a pitch-to-diameter ratio (P/D) of 3.0.

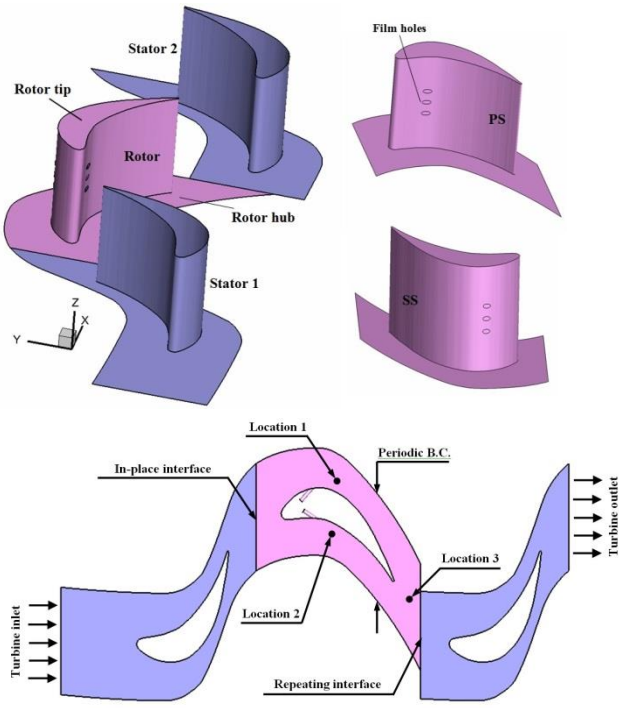

Fig. 1. Computational domain for 1-1/2 turbine stages.

The film hole is inclined 28° and 36° tangentially to the pressure side and suction side in the streamwise direction respectively. L/D, the length-to-diameter ratio of the film hole, is 3.15 for the pressure side and 3.95 for the suction side. S/D is the non-dimensional distance in the streamwise direction, where S is the surface distance downstream of the film hole. H/D is the non-dimensional distance in the spanwise direction.

BOUNDARY TREATMENTS AND FLOW CONDITIONS

The turbine stage inlet velocity (u_∞) and inlet total temperature (T_∞) are 30 m/s and 1800 K, respectively. The turbine stage inlet is defined as a velocity inlet with an inlet flow angle of 0°. A turbulence intensity of 2.7% and a turbulence length scale of 3% of the rotor chord length are applied at the turbine inlet. The flow outlet condition of the turbine stage is set as a pressure-outlet with the static pressure Pout=101325 Pa. The synthetic eddy method proposed by Jarrin et al. [29] was employed to provide turbulent eddies across inflow boundaries and provide an initial perturbated flow field at the inlet. The periodic boundary condition is imposed in the circumferential direction for both stators and rotor, as shown in Fig. 1. Relatively cooler air is employed as a coolant to protect the rotor surface from the hot mainstream. The coolant air is directly introduced into the film hole inlet sections by adopting a velocity inlet. The total temperature of the coolant flow (T_c) is taken to be $0.5T_\infty$, so that the coolant-to-mainstream density ratio DR= ρ_c/ρ_∞ is about 2.0, as in an engine, and the inlet velocity is determined according to the blowing ratio. Turbulent intensity at the film hole inlet is assumed to be 2.7%, while the turbulence length scale is taken to be 0.25D. The inlet of each film hole is defined as a velocity inlet, and the outlet is defined as an in-place interface between the rotor surface and the film hole exit. An adiabatic no-slip condition is applied for the solid wall boundaries of the stators, rotor and film holes.

GRID SYSTEM

Two multi-block grids were generated using POINTWISE software, one covering the 1-1/2 turbine stages and a second one inside the film holes. Detailed grid distribution is shown in Fig. 2. The domain of the 1-1/2 turbine stages was composed entirely of hexahedral meshes, which are more accurate with less numerical diffusion. The mesh was stretched away from the viscous wall using a stretching ratio of 1.15. A first height of 0.015 mm was used in order to accurately capture the boundary layer region. Near the leading and trailing edges of the blades, the grid was refined as dictated by the high-curvature regions of the leading and trailing edges. The second domain, on the other hand, consisted of two rows of film holes. Tetrahedral meshes were used in the film-hole domain since they are flexible to construct. These two meshes were then merged together to form a "hybrid" mesh, with a non-conformal interface boundary between them. For computational accuracy, the ratio of two adjacent grid sizes in any direction was kept within 0.87-1.15. No wall functions were used; thus viscous clustering was employed at all solid walls with a Y+ value of less than 1.0 for the first grid point off the wall at all locations. As the computational domain consists of rotating and stationary parts, interface boundaries are required between the rotating and stationary zones to interpolate the flow variables from the stationary zone to the rotating zone.

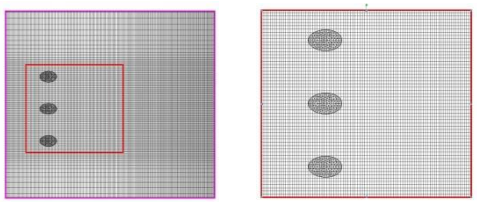

a) Grid structure on the suction surface shows three film holes.

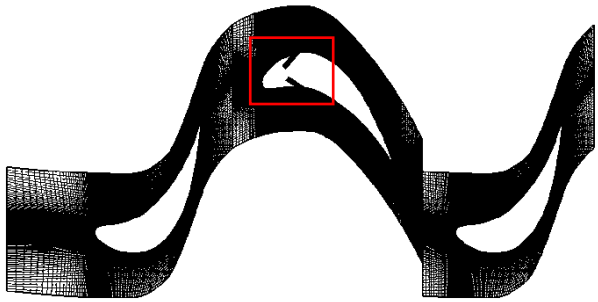

b) Grid structure for 1-1/2 turbine stages at mid-span plane .

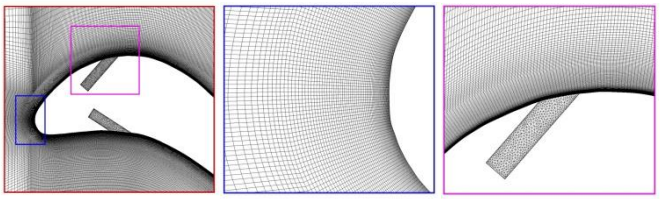

c) Grid structure for the leading edge of the rotor blade and for film cooling holes.

Fig.2 Numerical grids distribution for 1-1/2 turbine stages.

SPATIAL AND TEMPORAL RESOLUTION

Four grid topologies were adopted in this study to examine the grid sensitivity; the total numbers of the grids were 4,055,194, 8,507,418, 13,156,916, and 17,898,075. Note that the near-wall grid distance stays the same for these four sets of grids to keep the Y+ values less than 1.0. The effect of the grid size on the mid-span plane and spanwise-averaged film-cooling effectiveness distribution on both the suction and pressure surfaces was examined, as shown in Fig. 3. The figure indicates that there is no significant change in the film-cooling effectiveness when the grid size is increased above 13,156,916. Except in the case of S/D =2.1, and -3.0 points on the suction and pressure surfaces, respectively, increasing the total number of cells from 13,156,916 to 17,898,075, the local film-cooling effectiveness decreases by 3% on the suction surface for S/C=2.1 and increases by 2% on the pressure surface for S/D = -3.0. As a result of the above studies, the grid system with approximately 13 million cells was selected for computation. It consists of 2,035,264 million cells in stator 1 and stator 2

computational domains, 9,003,144 in that of the rotor with tip clearance, and 83,244 cells in the film holes.

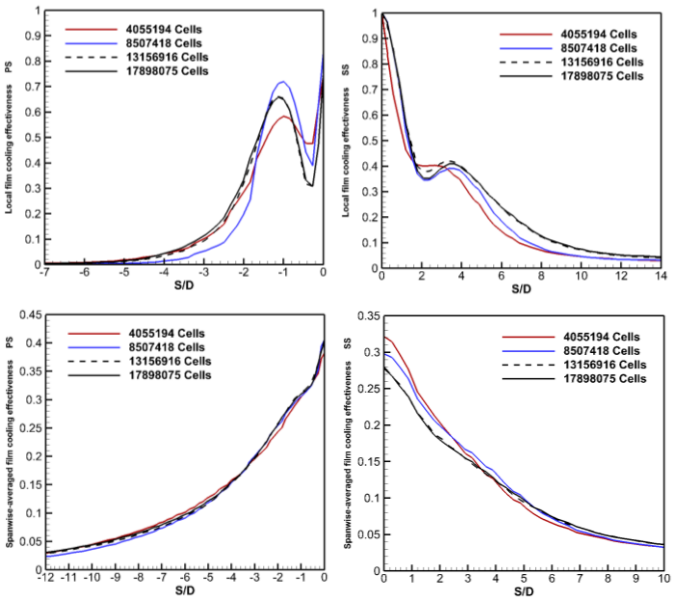

Fig. 3 Grid sensitivity study using the film-cooling effectiveness.

The time step is chosen in such a way that one passing period of the rotor blade is completed in 100 time steps. The passing period is defined as the time it takes for the rotor blade to move from one stator row to another. This corresponds to 1800 time steps to complete one full rotor-blade revolution. Since the maximum rotational speed is 2400 rpm and the number of rotor blades is 18, one revolution is completed in 2.5×10^{-2} s and, hence, the passing period is 1.39×10^{-3} s. As 100 time steps are used in calculating one passing period of the rotor blade, therefore, the time step is 1.39×10^{-5} s. This time step keeps the Courant Friedrichs Lewy (CFL) less than one for most of the flow field.

SOLUTION PROCEDURE

The simulations were carried out using the commercial CFD STAR-CCM+ code. Heat transfer and fluid flow characteristics were obtained by solving the flow-governing equations. The finite volume approach was used to discretise the partial differential equations (Eqs. 1-3) to yield a set of linear algebraic equations. The unsteady SIMPLE algorithm technique of Patankar and Spalding [30] was adopted for the velocity-pressure coupling. The WALE subgrid-scale model provided in the software was used to model turbulence, and the near-wall region was modelled using the low Y+ wall treatment option, which assumes that the viscous sublayer is resolved (since Y+ <1) and thus wall laws are not needed. The diffusive fluxes were approximated using second-order central differences. The convective terms were discretised using a bounded central-differencing scheme, as used by Leonard [31] and Darwish and Moukalled [32]. A full second-order implicit scheme of Ferziger and Peric [33] was applied for the temporal discretisation. This scheme uses the solution at the current time level as well as the solutions from the previous two time levels and is second-order accurate. The set of linearised equations was solved iteratively to find the flow variables, including the velocity, pressure, temperature and conserved scalars. This set of equations was then solved using the Gauss–Seidel method, which was coupled with an algebraic multigrid (AMG) solver to accelerate convergence.

VALIDATION OF THE COMPUTATIONAL METHOD

To validate the numerical method, the computational model was specified according to the experimental model configuration presented by Tao et al. [20] and Guoqing et al. [34]. The comparisons of the predicted spanwise-averaged film-cooling effectiveness with the measurements of Tao et al. [20] and Guoqing et al. [34] for various blowing ratios and Rt=0.0239 are shown in Fig. 4. The simulation and experiment were done with a single hole on the suction side and a single hole on the pressure side of the rotor blade.

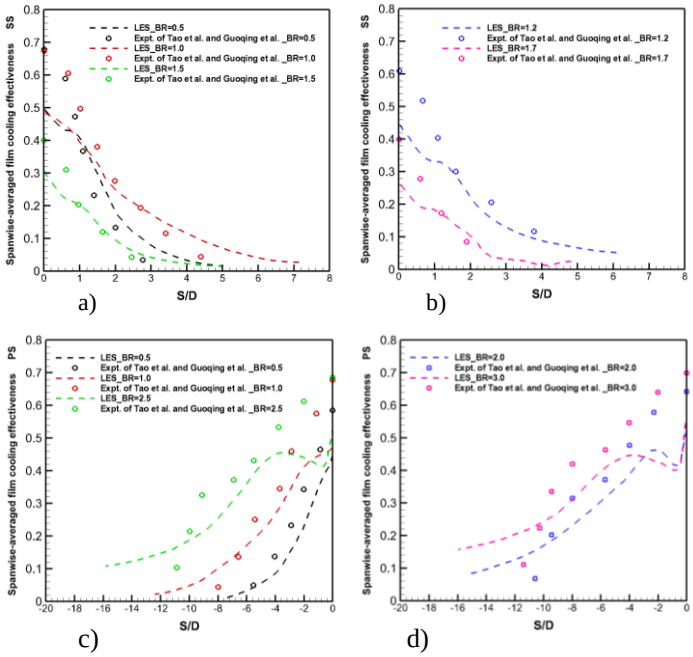

Fig. 4 Comparisons of the predicted spanwise-averaged film cooling effectiveness with the measurements of Refs. [20, 34] for various blowing ratio and Rt=0.0239.

It is clearly seen that the predicted effectiveness at hole position (S/D=0) is lower than that measured by Tao et al. and Guoqing et al. This mismatch could be due to the following three reasons. First, the spanwise-average value of η=0.6, which occurred at film hole position for many of the cases measured by Tao et al. and Guoqing et al., is much higher than would be expected. Consequently, the contour plots of film effectiveness in Tao et al. and Guoqing et al. were checked and found that these spatial distributions of η could not possibly result in spanwise-average values of η that were presented in their paper. Furthermore, the contour plots of the adiabatic wall temperature in Tao et al. and Guoqing et al. showed laterally spreading of coolant film at the hole position that is impossible. In short, film effectiveness results measured by Tao et al. and Guoqing et al. are not accurate. Second, the present study used

the inlet mainstream velocity of the turbine stage in the blowing ratio parameter, not the local mainstream velocity at the location of the film cooling holes. This is because the BR parameter must be defined prior to launching the numerical simulation, in this stage; the local mainstream values are unknown. However, the previous experimental studies [20, 34] were ambiguous about what was the mainstream velocity (inlet or local) used in the BR parameter. Third, to obtain a spanwise-average, Tao et al. and Guoqing et al. averaged the film effectiveness over the range ±3D near the centreline of the film trajectory. This is contrary to all other studies of film cooling, and makes it impossible to evaluate the significance of the performance of these film holes. In the present study, the predicted film effectiveness was averaged in the same field of ±3D but near the centreline of the film hole because it is difficult in terms of setting/numerical issues to average the effectiveness values near the centreline of the film trajectory.

On the other hand, however, downstream of the film hole, the predicted spanwise-averaged film-cooling effectiveness shows the same tendency as the experimental results. Fig. 4 (a & b) show that the numerical predictions agree with the experimental data at all blowing ratios on suction surface. On the pressure surface, Fig .4 (c) shows good agreement between the predictions and experiments at BR=0.5 and 1.0. For BR=2.0-3.0, the numerical prediction considerably under-predicts the cooling effectiveness, as shown in Fig. 4 (c and d).

RESULTS

The initialisation period and the statistically stationary state were monitored by the time history of the streamwise velocity and temperature at three different points in the computational domain. As mentioned earlier, one full rotor-blade revolution was completed in 1800 time steps. LES calculations were performed for 11,000 time steps (six full rotor blade revolutions) to reach the statistically stationary state. The simulations were run for another 14,000 time steps (seven full rotor blade revolutions) before beginning statistical sampling for the certainty of the stationary state and the solution integrity. Initially, mean flow variables (or the first-order statistics) were collected until they converged. As soon as the mean flow variable field has reached stable (time independent) values, the flow statistics (second-order statistics) can be calculated. Statistical samples were taken over a period of 45,000 time steps (25 full rotor blade revolutions).

The flow behaviour on the curved surfaces is strongly influenced by two opposing forces, namely the mainstream pressure gradient force and the centrifugal force. The mainstream pressure gradient force is generated by the pressure difference near the blade surfaces from that in the mainstream and the centrifugal force is generated by the surface curvature. On the pressure side, the pressure gradient pushes the flow away from the blade surface while the centrifugal force pushes it towards the blade surface. This means that the flow is under a favourable pressure gradient along the pressure side. Higher injection velocity results in stronger centrifugal force, which is good for the film attachment. Contrary to the pressure side, the mainstream pressure gradient pushes the flow towards the blade surface, while the centrifugal force pushes the flow away from the blade surface on the suction side, which strengthens the film detachment. Therefore, on the suction side, the flow is under an adverse pressure gradient.

FILM-COOLING PERFORMANCE ON THE PRESSURE SIDE

Fig. 5 shows the contours of the adiabatic wall temperature on the pressure side with varying blowing ratio. It can be seen that the film trajectory covers an area as small as 12D in streamwise direction at BR=1.0. At BR=2.0, the film coverage reaches 22D. The maximum film coverage occurs at BR=5.0, where it spans a length as long as 24D of the pressure surface streamwise. It can be concluded that the film coverage becomes longer with the increasing of blowing ratio. That means a higher blowing ratio generates greater film coverage, although the coolant with a higher blowing ratio lifts off the surface and penetrates into the mainstream. This behaviour is mainly because the flow on the pressure side experiences a favourable pressure gradient and centrifugal force effects, which are good for the film attachment. The flow with a higher velocity is drawn nearer to the wall than that with a lower velocity due to the effect of the centrifugal force. When the injection velocity is different, the strength of the centrifugal force is also different. Higher injection velocity leads to stronger centrifugal force. This force pushes the flow towards the wall on the concave surface so as to produce better film attachment. Therefore, the film coverage increases with an increase in the blowing ratio. The above comparison indicates that the coolant with a higher blowing ratio is beneficial for the film coverage on the pressure side.

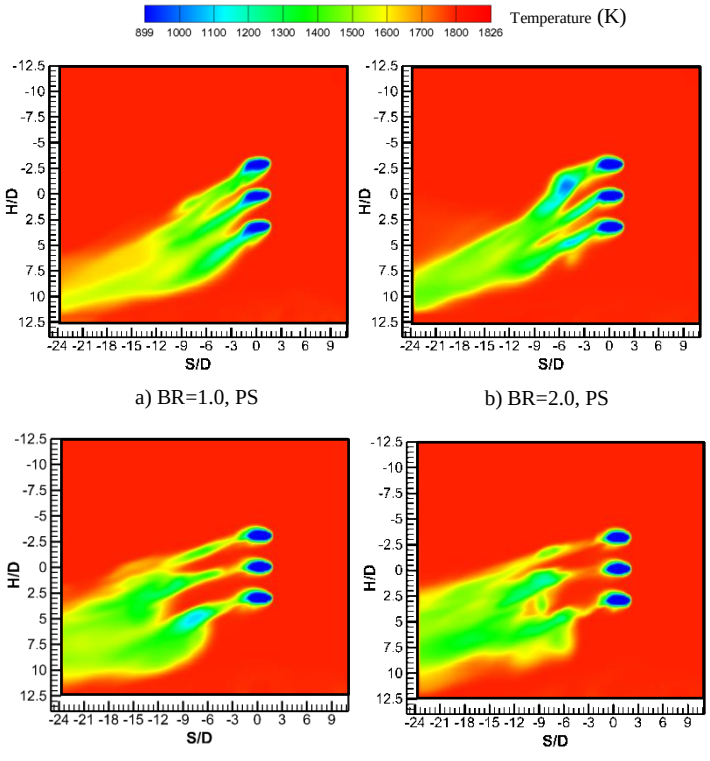

a) BR=1.0, PS b) BR=2.0, PS

c) BR=4.0, PS d) BR=5.0, PS

Fig. 5 Contours of the adiabatic wall temperature on the pressure side.

Fig. 6 presents the effect of the blowing ratio on the spanwise-averaged film-cooling effectiveness distribution in the streamwise direction. In the present study, the spanwise-averaged adiabatic film-cooling effectiveness ($\overline{\eta}$) was selected as the key parameter in representing the film-cooling performance, and was defined as:

$$\eta = \frac{T_\infty - < T_{aw} >}{T_\infty - T_c}$$

$$\overline{\eta} = \frac{\sum_{i=1}^{n} \eta_i A_i}{\sum_{i=1}^{n} A_i}$$

Where T_c is the coolant flow temperature, T_∞ is the mainstream temperature, T_{aw} is the adiabatic wall temperature at the blade surface, and n represents the number of nodes located in $\pm$ 9.0D at a certain streamwise location.

The case of the film-cooling effectiveness is similar to that of the film coverage. Near the film hole, $\overline{\eta}$ is highest at first due to the interaction of the coolant jet with the mainstream. Downstream of the film hole for each injection location, $\overline{\eta}$ decreases as S/D increases due to film dilution except for BR $\geq$ 2.0.

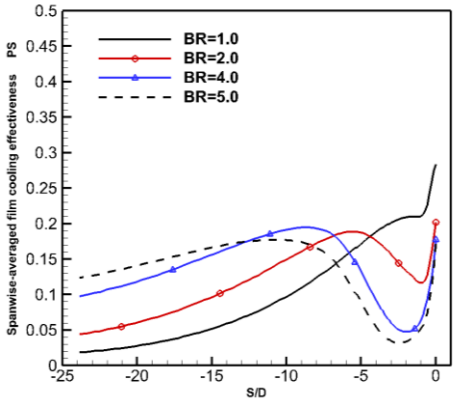

Fig. 6 Distributions of the spanwise-averaged film cooling effectiveness on the pressure surface with various blowing ratios.

For BR $\geq$ 2.0, $\overline{\eta}$ decreases until S/D=2.0 and then increases until S/D>6.0 due to the effect of the favourable pressure gradient and centrifugal force. Further downstream of the film hole at S/D $\geq$ 6.0, $\overline{\eta}$ decreases slightly for all values of BR ratio. It was found that there is a notable increase in film-cooling effectiveness from BR = 1.0 to BR = 5.0. $\overline{\eta}$ is about 0.025 (S/D is between 20 and 25) when BR is 1.0. When BR is increased to 2.0, $\overline{\eta}$ among S/D =20–25 is about 0.05, with a corresponding relative increase of 50%. Once BR is increased to 5.0, $\overline{\eta}$ among S/D =20–25 reaches 0.31, with a corresponding relative increase of 87%. This is a proof that film-cooling effectiveness increases with the blowing ratio.

For higher values of BR (BR $\geq$ 2.0), the film detaches from the surface due to the effect of the pressure gradient at S/D $\leq$ 2.0. The pressure side is a concave surface; therefore the near-wall pressure is higher than the mainstream pressure, which produces an accelerating pressure gradient capable of pushing the coolant flow away from the surface and disturbing the boundary layer. Further downstream of the film hole, the increase in mainstream velocity stabilises the boundary layer and the film reattaches to the surface due to the curvature effect (centrifugal force effect), which enables the coolant to cover the surface again. This is the reason why the film-cooling is more effective on the pressure side. As can be seen from Fig. 6, the film detachment occurs at S/D=1.0-2.0 downstream of the film hole when BR $\geq$ 2, and it then reattaches when S/D>2.0.

On the other hand, the film deflection can mainly be attributed to the effects of the Coriolis force and centrifugal buoyancy force. Under the rotational frame, these forces have a strong impact on the film-cooling distributions. Therefore, the Coriolis force and centrifugal buoyancy force determine whether the film trajectory bends centrifugally or centripetally. On the pressure side, rotation produces a centrifugal buoyancy force ($+\rho\Omega^2(r+z)\beta\Delta T$) towards the tip in the spanwise direction and a Coriolis force ($-2\rho\Omega v$) spanwise towards the hub. This means that these forces act in opposite directions. As the temperature difference between the coolant and mainstream is very high, the centrifugal buoyancy force will be stronger than the Coriolis force. As a result of this, the centrifugal buoyancy force plays a more important role in the film trajectory so that the film deflection acts centrifugally on the pressure side.

FILM-COOLING PERFORMANCE ON THE SUCTION SIDE

Fig. 7 shows the contours of the adiabatic wall temperature on the suction side with varying blowing ratio. On the suction side, the film coverage is different from that of the pressure side. The film covers only 10D and 18D in streamwise at BR=1.0 and 2.0, respectively. At BR=3.0, the film coverage reaches as far as 20D, which is 50 % further than that of BR=1.0. At BR = 4.0, the film coverage decreases to 18D. Therefore, the maximum coverage takes place at BR=3.0. This means that the film coverage is parabola with the rising of blowing ratio on the suction side. This behaviour because the flow on the suction side is situated in an adverse pressure gradient, which pushes the coolant to detach from the surface. Thus, the film-cooling performance on the pressure side is much better than that on the suction side. The maximum coverage of the pressure side is 1.47 times larger than that of the suction side in the streamwise direction.

The spanwise-averaged film-cooling effectiveness with varying blowing ratio is also compared in Fig. 8. The trend of the film-cooling effectiveness is nearly the same as the distributions of the film coverage but it is different from the pressure side. Near the film hole exit at S/D = 0.0, $\overline{\eta}$ can only reach 0.41 at BR=1.0, which is the highest in the whole range of blowing ratios investigated in this study on the suction surface. Then, $\overline{\eta}$ reduces to 0.37 at BR=2.0. Nearly in the middle of the film trajectory at S/D = 4.5, $\overline{\eta}$ = 0.12 at BR=1.0 and a higher value of 0.19 is achieved for BR=2.0. Further downstream of the film hole at S/D = 9.0, $\overline{\eta}$ = 0.04, 0.09, 0.1, 0.09 at BR=1.0, 2.0, 3.0 and 4.0, respectively. On the suction side, the film-cooling effectiveness increases with increasing blowing ratio at low blowing ratios and the maximum

magnitude occurs at a moderate blowing ratio of 2.0. After that, the film cooling effectiveness decreases with blowing ratio. Therefore, the film- cooling effectiveness is parabola with the increasing of blowing ratio on the suction side.

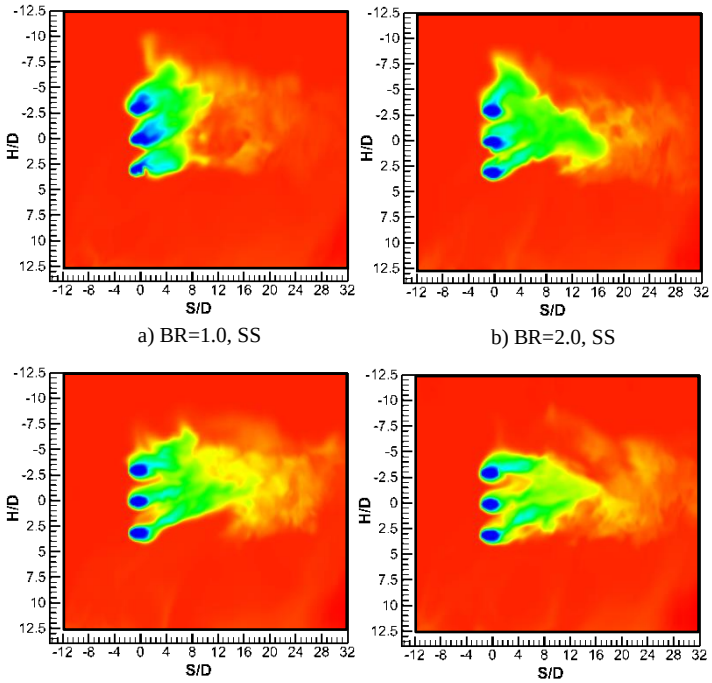

a) BR=1.0, SS b) BR=2.0, SS

c) BR=3.0, SS d) BR=4.0, SS

Fig. 7 Contours of the adiabatic wall temperature on the suction side.

On the suction side, the Coriolis force ($+2\rho\Omega v$) and centrifugal buoyancy force ($+\rho\Omega^2(r+z)\beta\Delta T$) generated by the rotation and temperature difference between the coolant and mainstream are both in the same spanwise direction towards the tip, while on the pressure side, the Coriolis force and centrifugal buoyancy force act in opposite directions. However, the effect of rotation on the pressure side is stronger than that on the suction side. This may be because of the curvature and adverse gradient pressure effects of the suction surface.

Fig. 9 presents the temperature distributions on the normal plane downstream of the film hole, where S denotes the distance between the normal plane and the centre of the film hole exit.

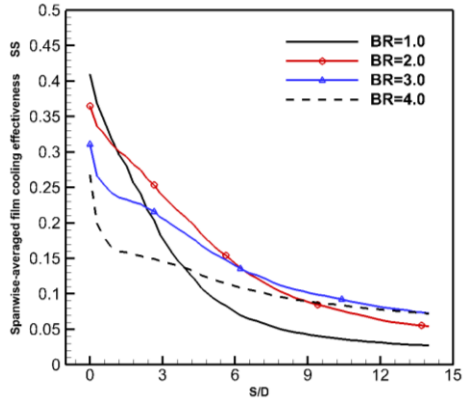

Fig. 8 Distributions of the spanwise-averaged film cooling effectiveness on the suction surface with various blowing ratios.

The interaction between the coolant jets and mainstream flow results in the formation of counter-rotating vortex pairs (CRVPs) and horseshoe vortices (HSVs). The presence of the CRVPs and HSVs causes the coolant jets to mix with the mainstream. The HSV, which wraps around the base of the coolant jet, remains close to the suction surface until it approaches the separation line of the end-wall boundary layer. The centres of the CRVPs, which result from the impulse of the coolant jet on the mainstream, move away from the surface in the Y–direction by moving away from the hole exit in streamwise direction. Also, the centres of the CRVPs move away from each other in spanwise direction. The mixing between the coolant and mainstream follows the development of the CRVPs and produces a variation in the density downstream of the hole exit.

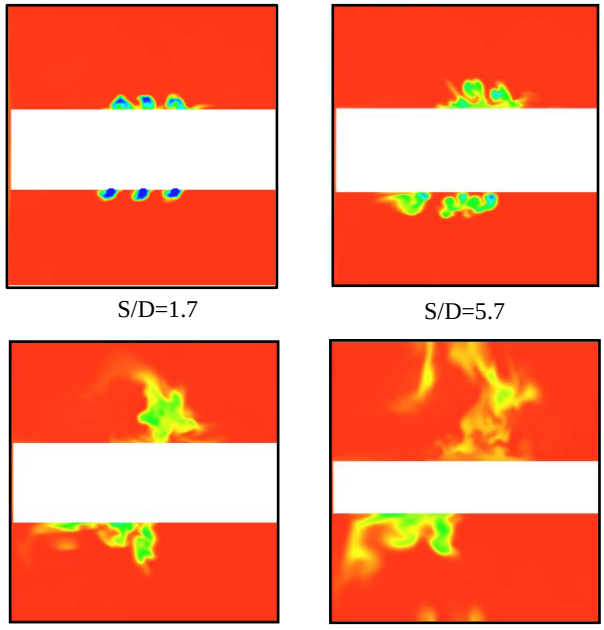

S/D=1.7 S/D=5.7

S/D=10.7 S/D=15.8

Fig. 9. Temperature contours on the normal plane downstream of film holes at BR= 4.0 (SS) and BR= 5.0 (PS).

These vortices then roll up the surface and, due to the shear between the coolant and the mainstream, continue to wrap and become larger as they move downstream. the CRVPs have a strong effect of pushing the flow towards the hub. Contrary to the centrifugal deflection on the pressure side, the jet trajectory always deflects centripetally on the suction surface. However, these forces tend to dominate the film movement in streamwise direction and disturb the CRVPs, as shown in Fig. 9.

CONCLUSION

The primary findings from this study are summarised as follows:

1. On the pressure side, the film coverage and film-cooling effectiveness increase as BR increases. The film deflection is weakened and the film attachment is strengthened as the blowing ratio increases. In other words, a lower blowing

ratio results in stronger film deflection. Film injection at a higher blowing ratio produces better film attachment. The flow is under a favourable pressure gradient along the entire pressure side.

2. On the suction side, the film coverage and film-cooling effectiveness increase with increasing blowing ratio at low blowing ratios but they decrease with a high blowing ratio. The film deflects centripetally on the suction side and the flow is under an adverse pressure gradient.

3. The coolant jets, which emanate from the film holes over the suction and pressure surfaces, disturb the boundary layer of the mainstream flow and increase the heat transfer downstream of the film holes. With increasing blowing ratio, the film coverage and film-cooling distribution are more uniform and the spanwise-averaged film-cooling effectiveness increases slightly.

4. Both rotation and blowing ratio play significant roles in determining the film-cooling effectiveness distribution along the rotor-blade surface. The film coverage and film-cooling effectiveness on the suction side are relatively smaller than those on the pressure side, possibly due to an adverse pressure gradient on the suction side pushing coolant towards the blade surface and a favourable pressure gradient on the pressure side pushing coolant away from the surface, which can be attributed to the curvature. The maximum film coverage on the pressure side is only 1.47 of that on the suction side. In addition, the centripetal film deflection on the suction side is very weak compare with the centrifugal film deflection on the pressure side.

REFERENCES

[1] S. Ito, R. J. Goldstein, and E. R. G. Eckert, "Film Cooling of a Gas Turbine Blade," *J. Eng. Power*, vol. 100, no. 3, pp. 476–481, 1978.

[2] N. W. Foster and D. Lampard, "The Flow and Film Cooling Effectiveness Following Injection through a Row of Holes," *J. Eng. Power*, vol. 102, no. 3, pp. 584–588, 1980.

[3] J. Andreopoulos and W. Rodi, "Experimental investigation of jets in a crossflow," *J. Fluid Mech.*, vol. 138, pp. 93–127, Jan. 1984.

[4] J. R. Pietrzyk, D. G. Bogard, and M. E. Crawford, "Hydrodynamic Measurements of Jets in Crossflow for Gas Turbine Film Cooling Applications," *J. Turbomach.*, vol. 111, no. 2, pp. 139–145, 1989.

[5] R. M. Kelso, T. T. Lim, and A. E. Perry, "An experimental study of round jets in cross-flow," *J. Fluid Mech.*, vol. 306, pp. 111–144, Jan. 1996.

[6] C. H. N. Yuen and R. F. Martinez-Botas, "Film cooling characteristics of rows of round holes at various streamwise angles in a crossflow: Part I. Effectiveness," *Int. J. Heat Mass Transf.*, vol. 48, no. 23–24, pp. 4995–5016, Nov. 2005.

[7] C. H. N. Yuen and R. F. Martinez-Botas, "Film cooling characteristics of rows of round holes at various streamwise angles in a crossflow: Part II. Heat transfer coefficients," *Int. J. Heat Mass Transf.*, vol. 48, no. 23–24, pp. 5017–5035, Nov. 2005.

[8] D. R. Pedersen, E. R. G. Eckert, and R. J. Goldstein, "Film Cooling With Large Density Differences Between the Mainstream and the Secondary Fluid Measured by the Heat-Mass Transfer Analogy," *J. Heat Transfer*, vol. 99, no. 4, pp. 620–627, 1977.

[9] S. S. Papell, "Vortex Generating Flow Passage Design For Increased Film-Cooling Effectiveness and Surface Coverage", Presented at the 22nd Natl. Heat Transfer Conf., Niagara Falls, N.Y., 5-8 Aug. 1984.

[10] J. R. Pietrzyk, D. G. Bogard, and M. E. Crawford, "Effects of Density Ratio on the Hydrodynamics of Film Cooling," *J. Turbomach.*, vol. 112, no. 3, pp. 437–443, 1990.

[11] A. K. Sinha, D. G. Bogard, and M. E. Crawford, "Film-Cooling Effectiveness Downstream of a Single Row of Holes With Variable Density Ratio," *J. Turbomach.*, vol. 113, no. 3, pp. 442–449, 1991.

[12] J. H. Leylek and R. D. Zerkle, "Discrete-Jet Film Cooling: A Comparison of Computational Results With Experiments," *J. Turbomach.*, vol. 116, no. 3, pp. 358–368, 1994.

[13] T. F. Fric and A. Roshko, "Vortical structure in the wake of a transverse jet," *J. Fluid Mech.*, vol. 279, pp. 1–47, Nov. 1994.

[14] K. B. M. Q. Zaman and J. K. Foss, "The effect of vortex generators on a jet in a cross-flow," *Phys. Fluids*, vol. 9, no. 1, pp. 106–114, 1997.

[15] D. K. Walters and J. H. Leylek, "A Detailed Analysis of Film-Cooling Physics: Part I—Streamwise Injection With Cylindrical Holes," *J. Turbomach.*, vol. 122, no. 1, pp. 102–112, 2000.

[16] J.C. Han, S. Dutta, and S. Ekkad, *Gas Turbine Heat Transfer and Cooling Technology*, 2nd edition. New York: Taylor & Francis, 2013.

[17] V. K. Garg, "Adiabatic effectiveness and heat transfer coefficient on a film-cooled rotating blade," *Numer. Heat Transf. Part A Appl.*, vol. 32, no. 8, pp. 811–830, Dec. 1997.

[18] V. K. Garg, "Heat transfer on a film-cooled rotating blade," *Int. J. Heat Fluid Flow*, vol. 21, no. 2, pp. 134–145, Apr. 2000.

[19] H. Yang, H.-C. Chen, J.-C. Han, and H.-K. Moon, "Numerical study of film cooled rotor leading edge with tip clearance in 1-1/2 turbine stage," *Int. J. Heat Mass Transf.*, vol. 51, no. 11–12, pp. 3066–3081, Jun. 2008.

[20] Z. Tao, G. Li, H. Deng, J. Xiao, G. Xu, and X. Luo, "Film cooling performance in a low speed 1.5-stage turbine: effects of blowing ratio and rotation," *J. Enhanc. Heat Transf.*, vol. 18, no. 5, pp. 419–432, 2011.

[21] N. Al-Zurfi and A. Turan, "LES of rotational effects on film cooling effectiveness and heat transfer coefficient in a gas

turbine blade with one row of air film injection," *Int. J. Therm. Sci.*, vol. 99, pp. 96–112, 2016.

[22] J.O. Hinze, *Turbulence*, 2nd edition. McGraw-Hill Book Company, New York, 1975.

[23] F. Nicoud and F. Ducros, ''Subgrid-Scale Stress Modelling Based on the Square of Velocity Gradient Tensor,'' Flow, Turbul. Combust., vol. 62, pp. 183–200, 1999.

[24] J. SMAGORINSKY, "GENERAL CIRCULATION EXPERIMENTS WITH THE PRIMITIVE EQUATIONS," *Mon. Weather Rev.*, vol. 91, no. 3, pp. 99–164, Mar. 1963.

[25] N. Al-Zurfi and A. Turan, "A Numerical Simulation of the Effects of Swirling Flow on Jet Penetration in a Rotating Channel," *Flow, Turbul. Combust.*, vol. 94, no. 2, pp. 415–438, Mar. 2015.

[26] N. Al-Zurfi and A. Turan, "A numerical study of rotation effects on jets effusing from inclined holes into a cross-flow," *J. Turbul.*, vol. 16, no. 11, pp. 1036–1057, Nov. 2015.

[27] N. Al-Zurfi and A. Turan, "LES of density ratio effects on film cooling under rotating frame," *Heat Mass Transf.*, vol. 52, no. 3, pp. 547–569, Mar. 2016.

[28] N. Al-Zurfi, A. Turan, and A. Nasser, "Numerical Investigation of Rotation Effects on Anti-vortex Film-Cooling Holes," *Flow, Turbul. Combust.*, vol. 96, no. 1, pp. 133–162, Jan. 2016.

[29] N. Jarrin, S. Benhamadouche, D. Laurence, and R. Prosser, "A synthetic-eddy-method for generating inflow conditions for large-eddy simulations," Int. J. Heat Fluid Flow, vol. 27, no. 4, pp. 585–593, Aug. 2006.

[30] S. Patankar and D. Spalding, "A calculation procedure for heat, mass and momentum transfer in three-dimensional parabolic flows," Int. J. Heat Mass Transf., vol. 15, no. 10, pp. 1787–1806, Oct. 1972.

[31] B. P. Leonard, "The ULTIMATE conservative difference scheme applied to unsteady one-dimensional advection," Comput. Methods Appl. Mech. Eng., vol. 88, no. 1, pp. 17–74, Jun. 1991.

[32] M. S. Darwish and F. H. Moukalled, "NORMALIZED VARIABLE AND SPACE FORMULATION METHODOLOGY FOR HIGH-RESOLUTION SCHEMES," Numer. Heat Transf. Part B Fundam., vol. 26, no. 1, pp. 79–96, Jul. 1994.

[33] J.H. Ferziger and M. Peric, *Computational Methods for Fluid Dynamics*, third ed. Springer, 2002.

[34] L. Guoqing, Z. Junqiang, D. Hongwu, T. Zhi, and L. Haiwang, "Experimental investigation of rotating film cooling performance in a low speed 1.5-stage turbine," *Int. J. Heat Mass Transf.*, vol. 61, no. 1, pp. 18–27, Jun. 2013.